J. Plasma Physics (1996), *vol.* ??, *part* ?, *pp.* ??–?? 1

Instability of magnetic modons and analogous Euler flows

By A.Y.K. CHUI AND H.K. MOFFATT

Department of Applied Mathematics and Theoretical Physics, University of Cambridge, Silver Street, Cambridge, CB3 9EW, UK

(Received 3 May 1996)

We construct numerical examples of a 'modon' (counter-rotating vortices) in an Euler flow by exploiting the analogy between steady Euler flows and magnetostatic equilibria in a perfectly conducting fluid. A numerical modon solution can be found by determining its corresponding magnetostatic equilibrium, which we refer to as 'magnetic modon'. Such an equilibrium is obtained numerically by a relaxation procedure which conserves the topology of the relaxing field.

Our numerical results show how the shape of a magnetic modon depends on its 'signature' (magnetic flux profile), and that these magnetic modons are unexpectedly unstable to non-symmetric perturbations. Diffusion can change the topology of the field through a reconnection process and separate the two magnetic eddies. We further show that the analogous Euler flow (or modon) behaves similar to a perturbed Hill's vortex.

1. Introduction

By exploiting the analogy between steady Euler flows and magnetostatic equilibria in a perfectly conducting fluid, Moffatt (1985) showed how the steady solutions of the Euler equation may be obtained by the means of magnetic relaxation. In this approach, an initial magnetic field with arbitrarily prescribed topology is allowed to relax in an incompressible, perfectly conducting but viscous fluid until a magnetostatic equilibrium is reached. For each magnetic field $\mathbf{B}$ satisfying the condition for magnetostatic equilibrium

$$\mathbf{j} \wedge \mathbf{B} = \nabla p\,, \tag{1.1}$$

where $\mathbf{j} = \nabla \wedge \mathbf{B}$ is the current density and p is the fluid pressure, there corresponds a velocity field $\mathbf{u}$ satisfying the steady Euler equation

$$\mathbf{u} \wedge \boldsymbol{\omega} = \nabla h\,, \tag{1.2}$$

where $\boldsymbol{\omega} = \nabla \wedge \mathbf{u}$ is the vorticity and $h = p/\rho + \frac{1}{2}u^2$, via the analogy

$$\mathbf{B} \leftrightarrow \mathbf{u}\,, \quad \mathbf{j} \leftrightarrow \boldsymbol{\omega}\,, \quad p_0 - p \leftrightarrow h\,. \tag{1.3}$$

Magnetic relaxation can therefore be used as a means to obtain steady Euler flows with prescribed topology.

This technique is exploited in this paper in order to construct numerical examples of a 'modon' (a pair of propagating counter-rotating vortices). In a frame that moves with the modon, the flow is a steady solution of the Euler equation, having a pair of stationary vortices embedded in a uniform, steady background flow. A modon then corresponds (via the analogy 1.3) to magnetostatic equilibrium of a magnetic dipolar structure, which we shall here describe as a 'magnetic modon'. Such an equilibrium is obtained numerically by a relaxation procedure (see § 2 below) which conserves the topology of the relaxing field.

The only known analytic solution (sometimes referred to as the Lamb-Batchelor modon) is obtained by solving

$$\nabla^2\psi = -k^2\psi \tag{1.4}$$

in a circle of radius r_0, where ψ is the streamfunction of the flow, and matching the boundary condition to a uniform flow past a cylinder. The solution is

$$\psi = \psi_0 = \begin{cases} J_1(kr)\sin\theta\,, & \text{when } r < r_0; \\ \frac{k}{2}J_0(kr_0)\left(r - \frac{r_0^2}{r}\right)\sin\theta, & \text{when } r \geq r_0, \end{cases} \tag{1.5}$$

where J_0 and J_1 are Bessel functions, and k is the smallest positive number satisfying $J_1(kr_0) = 0$. In general, the streamfunction of a non-circular modon satisfies the Grad-Shafranov equation

$$\nabla^2\psi = F(\psi) \tag{1.6}$$

where F is an arbitrary function which, indirectly, describes the circulation distribution of the rotational fluid. Either F or the shape of the modon, but not both, can be specified in numerical calculations (see, for example, Boyd & Ma 1990, Eydeland & Turkington 1988).

Two cases of non-circular magnetic modons are here studied in detail: (A) the magnetic field is weak near the centre of each magnetic eddy; (B) the magnetic field is strong near the centre of each eddy. In § 2, we present details of the magnetic relaxation process. In each case, the magnetic field rapidly reaches a near-equilibrium state in which the eddies are elongated, but is then unexpectedly unstable to non-symmetric perturbations. In § 3, we consider the Euler flows that are analogous to the near-equilibrium states and follow their subsequent time-dependent evolution. In particular, we examine how the modons response to non-symmetric perturbations. Some physical explanations to the numerical results are given in § 4.

2. Magnetic relaxation

2.1. *Governing equations*

In magnetic relaxation, a suitable initial magnetic field is allowed to relax in an incompressible, perfectly conducting but viscous fluid. Magnetic field lines are frozen in such a fluid, and the energy

$$\mathcal{M} = \frac{1}{2}\int \mathbf{B}^2 \mathrm{d}V \tag{2.1}$$

is dissipated whenever the fluid is in motion, so an equilibrium state topologically accessible from the initial field and of minimum energy will be reached.

Any dynamical model which dissipates energy but conserves magnetic field topology may be adopted. We use here a quasi-static 'porous medium' dynamical law, so that the governing equations are:

$$k\mathbf{u} = -\nabla p + \mathbf{j}\wedge\mathbf{B}\,,$$

$$
\begin{aligned}
\frac{\partial \mathbf{B}}{\partial t} &= \nabla \wedge (\mathbf{u} \wedge \mathbf{B})\,, \\
\nabla \cdot \mathbf{B} &= 0\,, \\
\nabla \cdot \mathbf{u} &= 0\,,
\end{aligned}
\tag{2.2}
$$

where $k > 0$. Rigid-wall boundary conditions $\mathbf{u} \cdot \mathbf{n} = 0$, $\mathbf{B} \cdot \mathbf{n} = 0$ (or periodic boundary conditions) are assumed. It follows that

$$
\begin{aligned}
\frac{\mathrm{d}\mathcal{M}}{\mathrm{d}t} &= \int \mathbf{B} \cdot \frac{\partial \mathbf{B}}{\partial t}\,\mathrm{d}V = \int \mathbf{B} \cdot \nabla \wedge (\mathbf{u} \wedge \mathbf{B})\,\mathrm{d}V \\
&= \int \nabla \wedge \mathbf{B} \cdot \mathbf{u} \wedge \mathbf{B}\,\mathrm{d}V = \int \mathbf{u} \cdot \mathbf{B} \wedge \mathbf{j}\,\mathrm{d}V \\
&= \int \mathbf{u} \cdot (-\nabla p - k\mathbf{u})\,\mathrm{d}V = -k \int \mathbf{u}^2\,\mathrm{d}V < 0\,,
\end{aligned}
\tag{2.3}
$$

so that the energy decreases whenever the fluid is in motion.

For two-dimensional fields, we define the flux function χ for $\mathbf{B}$ and the stream-function ψ for $\mathbf{u}$ by (in Cartesian coordinates)

$$
\begin{aligned}
\mathbf{B} &= \nabla \wedge (\chi\,\hat{\mathbf{z}})\,, \\
\mathbf{u} &= \nabla \wedge (\psi\,\hat{\mathbf{z}})\,,
\end{aligned}
\tag{2.4}
$$

so that $(2.2\,c,d)$ are always satisfied, and $(2.2\,a,b)$ become

$$
\begin{aligned}
\frac{\partial \chi}{\partial t} &= J(\psi, \chi)\,, \\
\nabla^2 \psi &= -J(\chi, \nabla^2 \chi)\,,
\end{aligned}
\tag{2.5}
$$

where J is the usual Jacobian operator defined by $J(f,g) = f_x g_y - f_y g_x$. Numerical integration is performed on a uniform rectangular grid in the domain ($-a < x < a$, $-b < y < b$) with rigid-wall boundary conditions on $y = \pm b$,

$$
\psi(x, \pm b) = \mathrm{cst.}\,, \quad \chi(x, \pm b) = \mathrm{cst.}\,, \tag{2.6}
$$

and periodic boundary conditions at $x = \pm a$,

$$
\psi(-a, y) = \psi(a, y)\,, \quad \chi(-a, y) = \chi(a, y)\,. \tag{2.7}
$$

2.2. *Initial data*

The initial magnetic field must satisfy two criteria: (1) it has the same topology as that of a magnetic modon; (2) the boundary condition $\mathbf{B} \cdot \mathbf{n} = 0$ is satisfied at $y = \pm b$. Let χ_0 be the vector potential of a circular magnetic (Lamb-Batchelor) modon, normalized via (cf. 1.5)

$$
\chi_0 = \frac{\psi_0}{\max_{r<r_0} |\psi_0|}\,, \tag{2.8}
$$

so that the maximum value of χ_0 inside the magnetic eddies is 1. Let

$$
\chi_1 = \begin{cases} f(\chi_0)\,, & \text{when } r < r_0; \\ f'(0)\chi_0\,, & \text{when } r \geq r_0, \end{cases} \tag{2.9}
$$

where f is any monotonic increasing function with the properties $f(0) = 0$ and $f(1) = 1$. Note that (i) χ_1 and χ_0 have the same topology because the function f simply re-labels the field lines, and (ii) the 'speed of the flow', $|\nabla \chi_1|$, is continuous

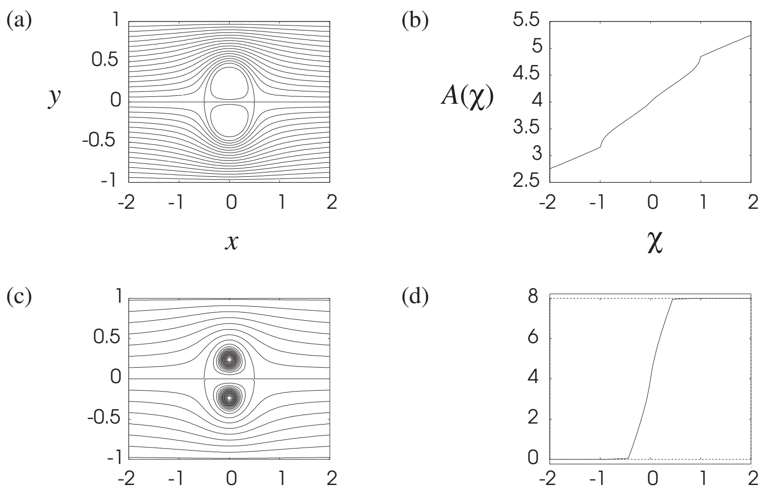

FIGURE 1. The initial magnetic fields: (*a*) the contour plot of the flux function χ_A defined in Case A; (*b*) the signature function of χ_A; (*c*) the contour plot of the flux function χ_B defined in Case B; (*d*) the signature function of χ_B.

across the boundary of the rotational region. However, χ_1 does not 'fit' in the rectangular domain because it does not satisfy $\mathbf{B}\cdot\mathbf{n}=0$ on $y=\pm b$.

In order to construct a field that does satisfy this boundary condition, we modify the field χ_1 as follows. Let χ_2 be a uniform magnetic field defined by

$$\chi_2 = Ky \tag{2.10}$$

where

$$K = \frac{k}{2} f'(0) J_0(kr_0)\,. \tag{2.11}$$

Note that $\chi_1 \to \chi_2$ as $r\to\infty$. We mix the fields χ_1 and χ_2 via

$$\chi_3 = \lambda\chi_1 + (1-\lambda)\chi_2\,, \tag{2.12}$$

where λ is a weight function that tends to 0 on the sides of the rectangle and tends to 1 at the centre (the origin). A suitable choice of λ is

$$\lambda = \cos\left(\frac{\pi x^2}{2a^2}\right)\cos\left(\frac{\pi y^2}{2b^2}\right). \tag{2.13}$$

Then

$$\chi_3(x,\pm b) = \pm Kb \tag{2.14}$$

so that the boundary condition $\chi_3=$ cst. (hence $\mathbf{B}\cdot\mathbf{n}=0$) is satisfied.

In this paper, we consider two cases of non-circular magnetic modons: (A) the magnetic field is weak near the centre of each magnetic eddy; (B) the magnetic field is strong near the centre of each eddy. For Case A, we choose $f(\chi_0) = \tanh(4\chi_0)/\tanh(4)$, so that

$$\chi_3 = \chi_A \stackrel{\text{def}}{=} \begin{cases} \lambda\tanh(4\chi_0)/\tanh(4) + (1-\lambda)K_a y\,, & \text{when } r<r_0;\\ 4\lambda\chi_0/\tanh(4) + (1-\lambda)K_a y\,, & \text{when } r\geq r_0, \end{cases} \tag{2.15}$$

where $K_a = 2kJ_0(kr_0)/\tanh(4)$. For Case B, we choose $f(\chi_0)=\chi_0(1+5\chi_0^4)/6$, so that

$$\chi_3 = \chi_B \stackrel{\text{def}}{=} \begin{cases} \frac{1}{6}\lambda\chi_0\left(1+5\chi_0^4\right) + (1-\lambda)K_b y\,, & \text{when } r < r_0; \\ \frac{5}{6}\lambda\chi_0 + (1-\lambda)K_b y\,, & \text{when } r \geq r_0. \end{cases} \tag{2.16}$$

where $K_b = kJ_0(kr_0)/12$. The contour plots of χ_A and χ_B are shown in Figures 1a & 1c. Figures 1b & 1d show the *signature functions* $A(\chi)$ of the two fields, where $A(\chi_c)$ is the total area of the regions in which $\chi \leq \chi_c$. These signature functions are estimated using bilinear interpolation on the mesh data. During the relaxation, the signature function of the magnetic field should be an invariant Moffatt (1986a).† Computing the signature function therefore provides a means of monitoring the accuracy of the numerical simulation.

2.3. *Numerical results*

Numerical simulations have been performed on meshes with various sizes: 129×65, 257×65 and 257×129. A finite difference method is used. Derivatives are approximated by standard formulae up to third order, and the Runge-Kutta (4th order) method with variable time steps is used for time-stepping. Linardatos (1993) reported some magnetic relaxation calculations for magnetic fields with single elliptic point. We tested our code on those magnetic fields; the equilibrium states we obtained are in excellent agreement with those of Linardatos.

We first present the results for χ_B (Case B) calculated on a 129×65 mesh equally spaced in the rectangular region $(-2 < x < 2,\ -1 < y < 1)$. The radius of the rotational region, r_0, is set to $1/2$. In Figure 2a, the magnetic energy is plotted against the time. The magnetic energy rapidly decreases from 4.026 (when $t = 0$) to 3.795 (when $t = 0.1$); the field evolves towards an equilibrium state (see Figure 2b) while the magnetic energy tends to a stationary value. The signature function is invariant during the relaxation process at expected. The shape of the modon changes from a circle to an oval with the longer axis parallel to the y-axis. The change in the shape has two effects: (1) it allows more room for each eddy to become more circular, hence the energy contributed by the eddies decreases; (2) it pushes some field lines towards the edges of the channel, hence the energy contributed by the background field increases. The equilibrium state achieves a dynamical balance between these two effects.

In Figure 2d, $\nabla^2\chi$ is plotted against χ at the initial state; each point in the plot corresponds to a $(\nabla^2\chi, \chi)$-pair evaluated at a mesh point on the rectangular grid. The points are scattered as expected since the initial state is not at equilibrium. Figure 2e shows the scatterplot of $\nabla^2\chi$ against χ in the final state. A functional relationship of the form (1.6) between $\nabla^2\chi$ and χ is evident; the final state is therefore very close to a magnetostatic equilibrium.

A surprising result is found for Case A. Figure 3 shows a sequence of contour plots illustrating how the magnetic modon may disappear in a rapid reconnection process. Those results are calculated on a 257×129 mesh in the rectangular region $(-2 < x < 2, -1 < y < 1)$. The magnetic modon stays at a near-equilibrium (symmetric about the x-axis) for a long period, then there is a symmetry-breaking instability (presumably triggered by random numeric noise) which tilts the modon. Once the modon is tilted, the two saddle points collapse to Y-points (cf. Linardatos 1993)

† In Moffatt (1986a), the signature of a field $A(\chi)$ is defined as the area enclosed by the closed field line with label χ. Here we extend the definition of the signature (as in the text) so that $A(\chi)$ is always defined even if the field lines are not closed.

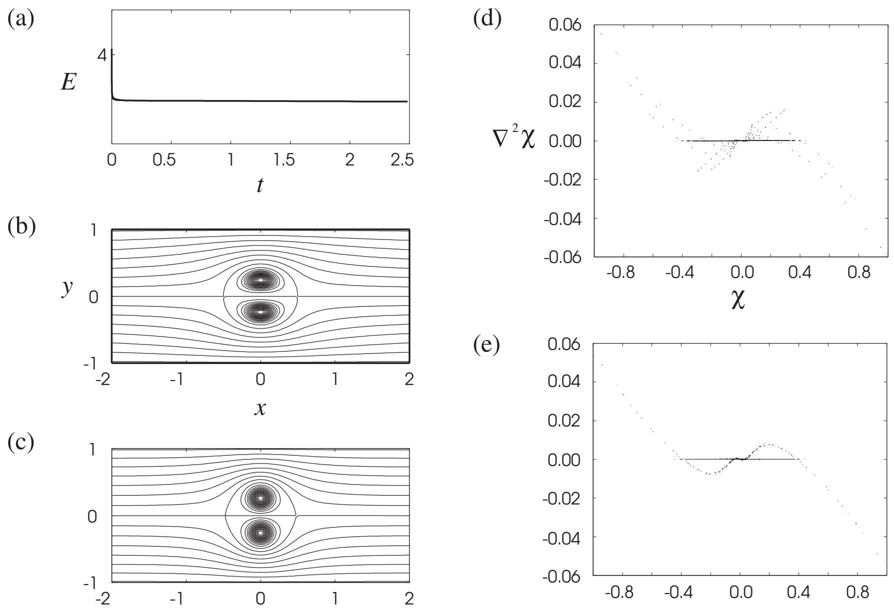

FIGURE 2. The magnetic relaxation of χ_B (Case B): (*a*) the energy quickly approaches a minimum value; (*b*) the initial state to be relaxed; (*c*) the final state of minimum energy; (*d*) the $(\nabla^2\chi, \chi)$ scatterplot at the initial state; (*e*) the $(\nabla^2\chi, \chi)$ scatterplot at the final state showing the functional relationship between $\nabla^2\chi$ and χ.

with associated current sheets. Due to unavoidable numerical diffusivity, reconnection occurs and quickly annihilates the eddies. Figure 3a shows how the energy changes with time; the plot shows clearly how rapidly the reconnection takes place when compared with the relatively long life-time of the near-equilibrium state. We note an interesting phenomenon observed from the numerical results: the signature function is invariant (up to the accuracy of the estimate) throughout the relaxation process even though the rapid reconnection has occurred (see footnote in §2.2).

To see how close the near-equilibrium state is to the actual symmetric equilibrium state, we present scatterplots of $\nabla^2\chi$ against χ in Figure 4. The functional relationship is evident in Figure 4b but not as good as that in Case B; the loss of accuracy is perhaps due to the steep gradient of the vector potential χ_A near the boundaries of the eddies.

It is puzzling why the magnetic modon is stable in one case but not in the other. We therefore re-examine Case B by extending the integration time; the magnetic modon appears to remain stable. However, if a small non-symmetric perturbation is added to the initial state, then a non-symmetric instability is found. Figure 5 shows the numerical results and it is evident that the behaviour is similar to Case A. It becomes clear that non-symmetric instability can occur in both cases; the growth rate of the instability in Case B is, however, much smaller than that in Case A.

We shall discuss these results again in §4. In the next section, we consider the time-dependent behaviour of the analogous Euler flows.

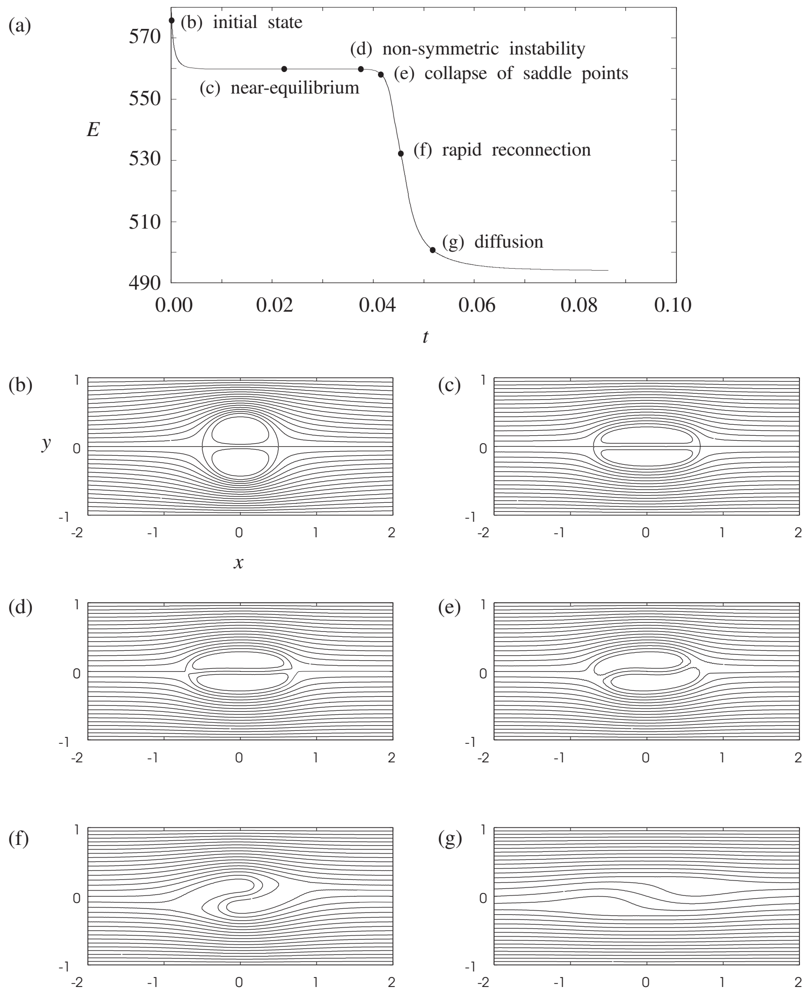

FIGURE 3. The magnetic relaxation of χ_A (Case A): (a) the energy is plotted against the time, showing a slow phase of near-equilibrium and a rapid phase of magnetic reconnection; (b-g) 'snap-shots' of the magnetic field at various stages (each represented by a dot on the energy plot (a).

3. Analogous Euler Flows

Even when the magnetostatic equilibria obtained by a relaxation procedure are stable, the analogous Euler flows may be unstable. The analogy applies only to the structure of the steady states, but not to their stability properties Moffatt (1986b). Only in very special cases can we prove the stability of the analogous Euler flows (see Davidson 1994). We investigate here the behaviour of the analogous Euler flows using the near-equilibrium states obtained in the previous section.

We adopt the Euler equation in the form

$$\frac{\partial \omega}{\partial t} = J(\psi, \omega)$$

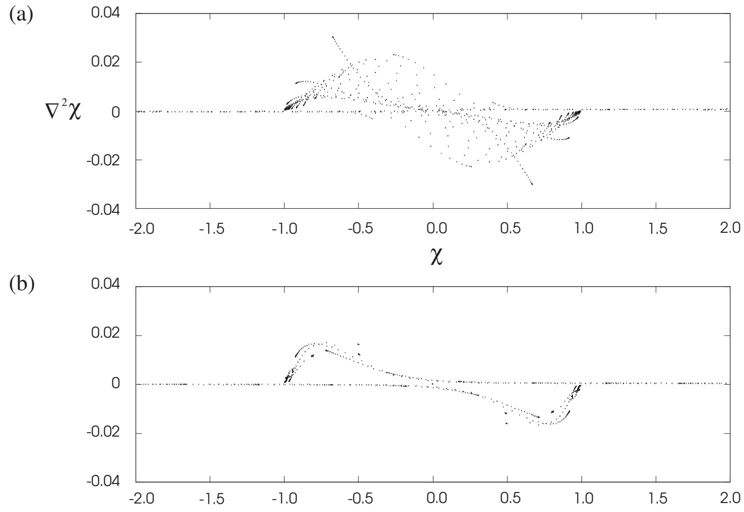

FIGURE 4. The $(\nabla^2\chi, \chi)$ scatterplot in (*a*) the initial state and (*b*) the final state. The functional relationship between $\nabla^2\chi$ and χ is still evident in (b).

where $\omega = -\nabla^2\psi$. A simple implementation of a finite difference method (2nd order accurate) with fixed grid size is used. We use a special formula (Arakawa 1966) to evaluate the Jacobian so that the enstrophy, $\int \omega^2 \mathrm{d}V$, is conserved. This refinement makes prolonged numerical integration more stable. However, our results are still only a rough approximation to the truth because our method cannot resolve the fine scales that develop naturally under Euler evolution.

Figure 6 shows the behaviour of the near-equilibrium state in Case A under Euler dynamics. The fluid is moving from left to right. The integration continued till $t \approx 0.6$ and snap-shots of the evolution up to $t = 0.3628$ are shown in Figure 6b; the modon can propagate 6 times its own width during this period. We found that the disturbances are swept in the downstream direction. This kind of response is found also in a perturbed Hill's vortex (Moffatt & Moore 1978, Pozrikidis 1986), except that the spike of rotational fluid found by Pozrikidis (accumulating at the rear stagnation point) cannot be observed in our simulation. We monitored the kinetic energy and the enstrophy of the fluid: over this time of integration, they vary within 1% of their initial values (Figure 6a). Careful examination of the data shows, however, that the maximum value of $|\omega|$ within each vortex has increased by 100%; the (false) gain of vorticity inside the rotational region is due to an accumulation of truncation error in prolonged numerical integration.

We speculate that the modon would response to disturbance in a similar way if this false gain of vorticity could have been suppressed. However, developing a more accurate unsteady Euler equation solver is beyond the scope of this paper.

It is interesting to test how the near-equilibrium state responds to non-symmetric perturbation. Figure 7 shows how quickly the modon breaks down (near $t = 0.06$)). The change of topology is due to the unavoidable numerical viscosity.

Similarly, Figure 8 shows how the near-equilibrium state in Case B behaves under Euler dynamics, and Figure 9 shows how the near-equilibrium state responds to non-

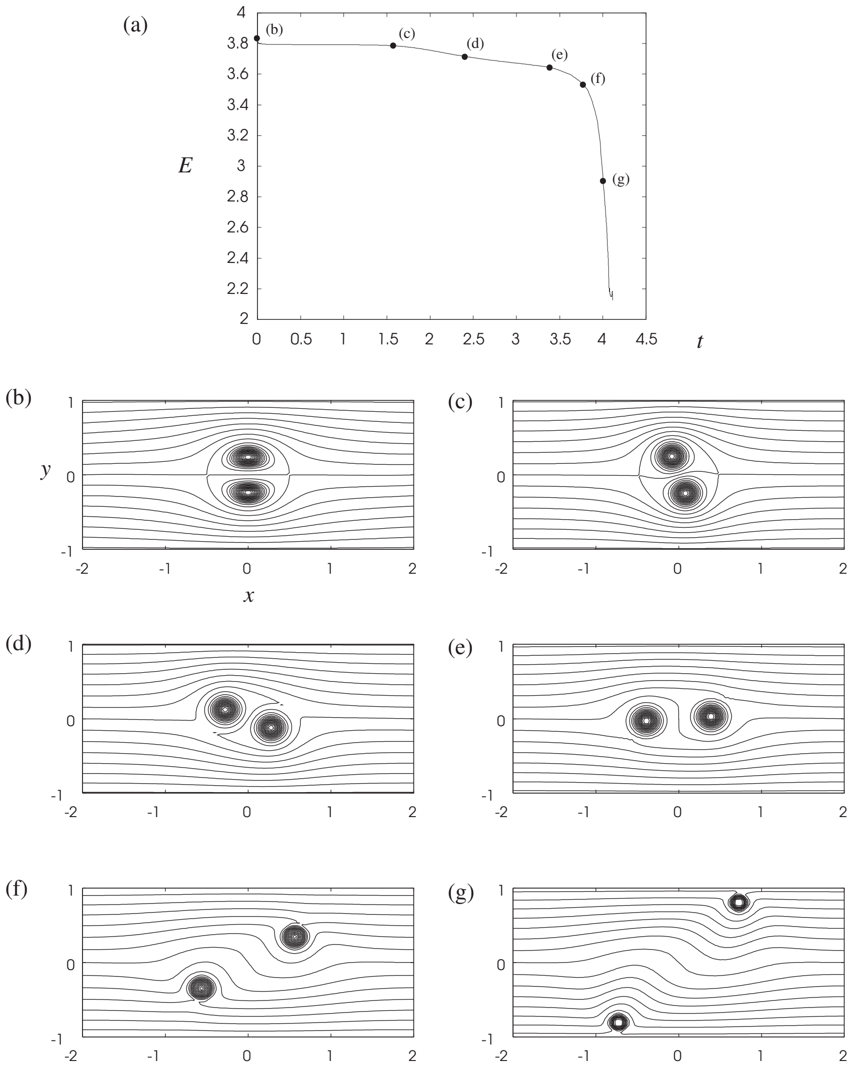

FIGURE 5. The magnetic relaxation of perturbed χ_B: (a) the energy is plotted against the time, showing a slow phase of near-equilibrium and a rapid phase of magnetic reconnection; (b-g) the 'snap-shot' of the magnetic field at various stages (each represented by a dot on the energy plot (a)).

symmetric disturbances. The results suggest that the modon initially oscillates, then irrotational fluid enters the modon near the rear stagnation point, and finally the modon moves away from the centred position. An interesting feature is that the modon does not break up during the evolution. Again, this behaviour needs to be verified by a more accurate numerical scheme in future research.

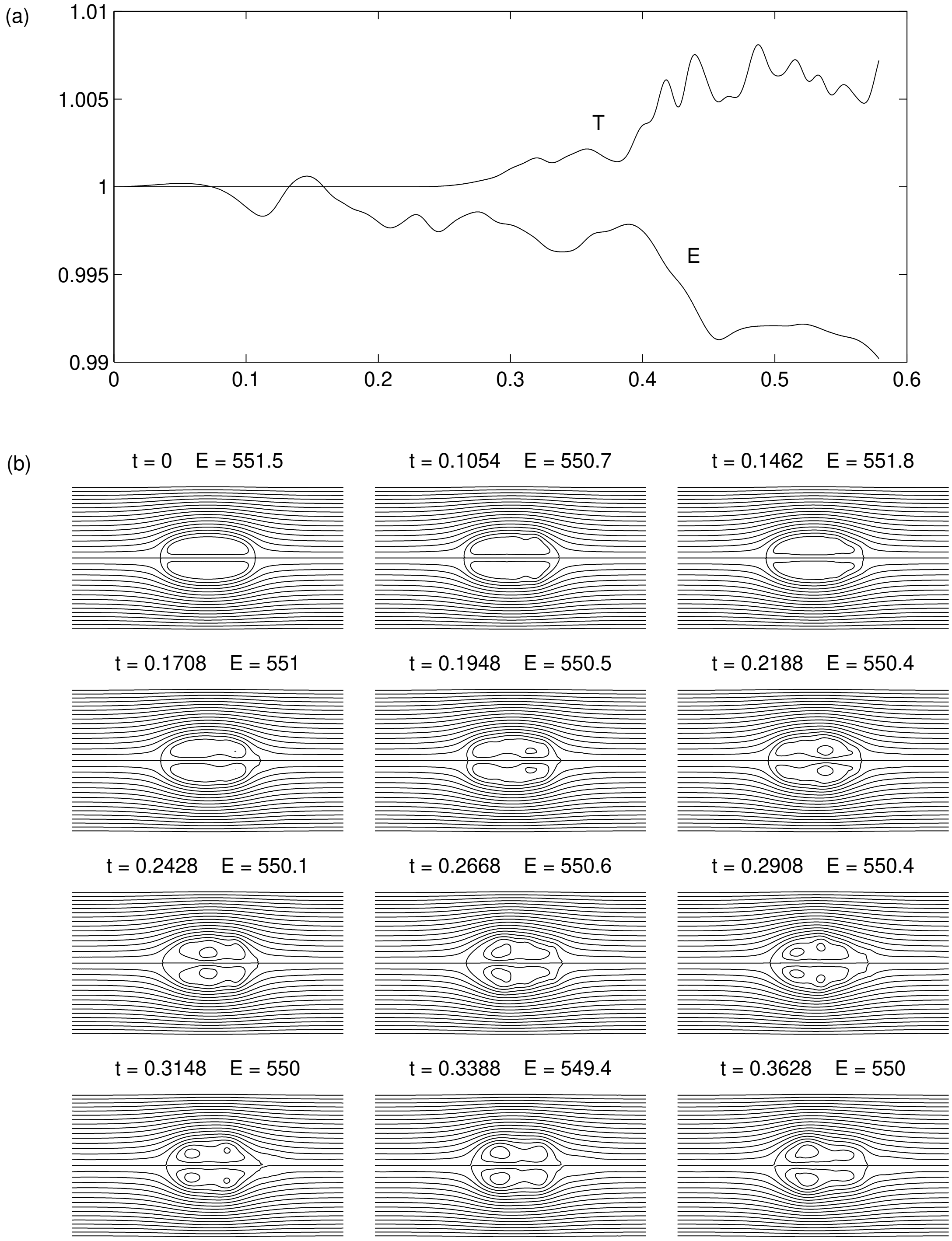

FIGURE 6. The behaviour of the near-equilibrium state in Case A under the Euler dynamics: (a) the kinetic energy E and the enstrophy T vary within 1% of their initial values; (b) the snap-shots show that the modon behaves like a perturbed Hill's vortex.

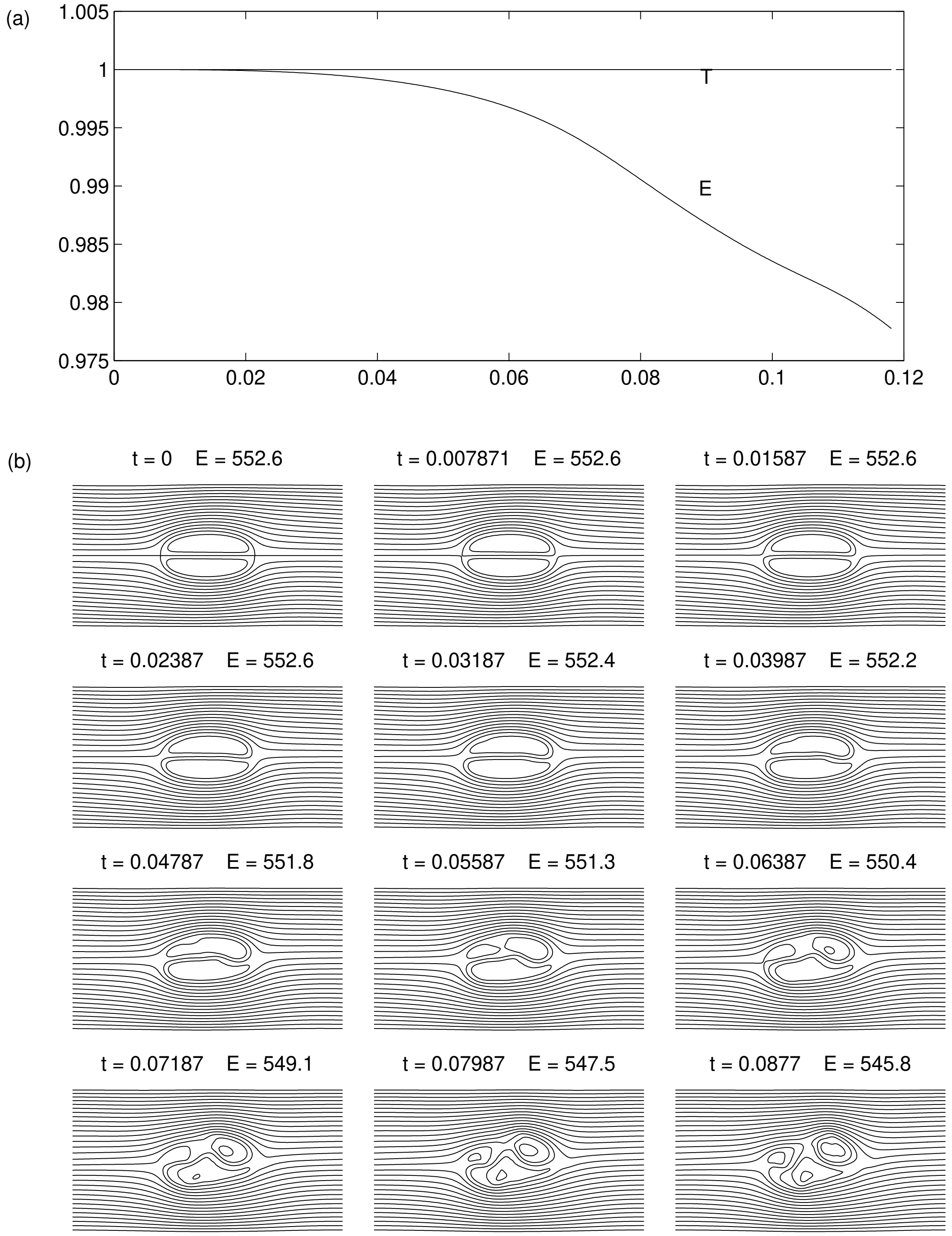

FIGURE 7. When a small non-symmetric perturbation is applied to the the near-equilibrium state in Case A, the modon breaks down quickly under the Euler dynamics. (a) The kinetic energy E and the enstrophy T vary within 2.5% of their initial values; (b) the snap-shots show how rapidly the modon responds to non-symmetric perturbations.

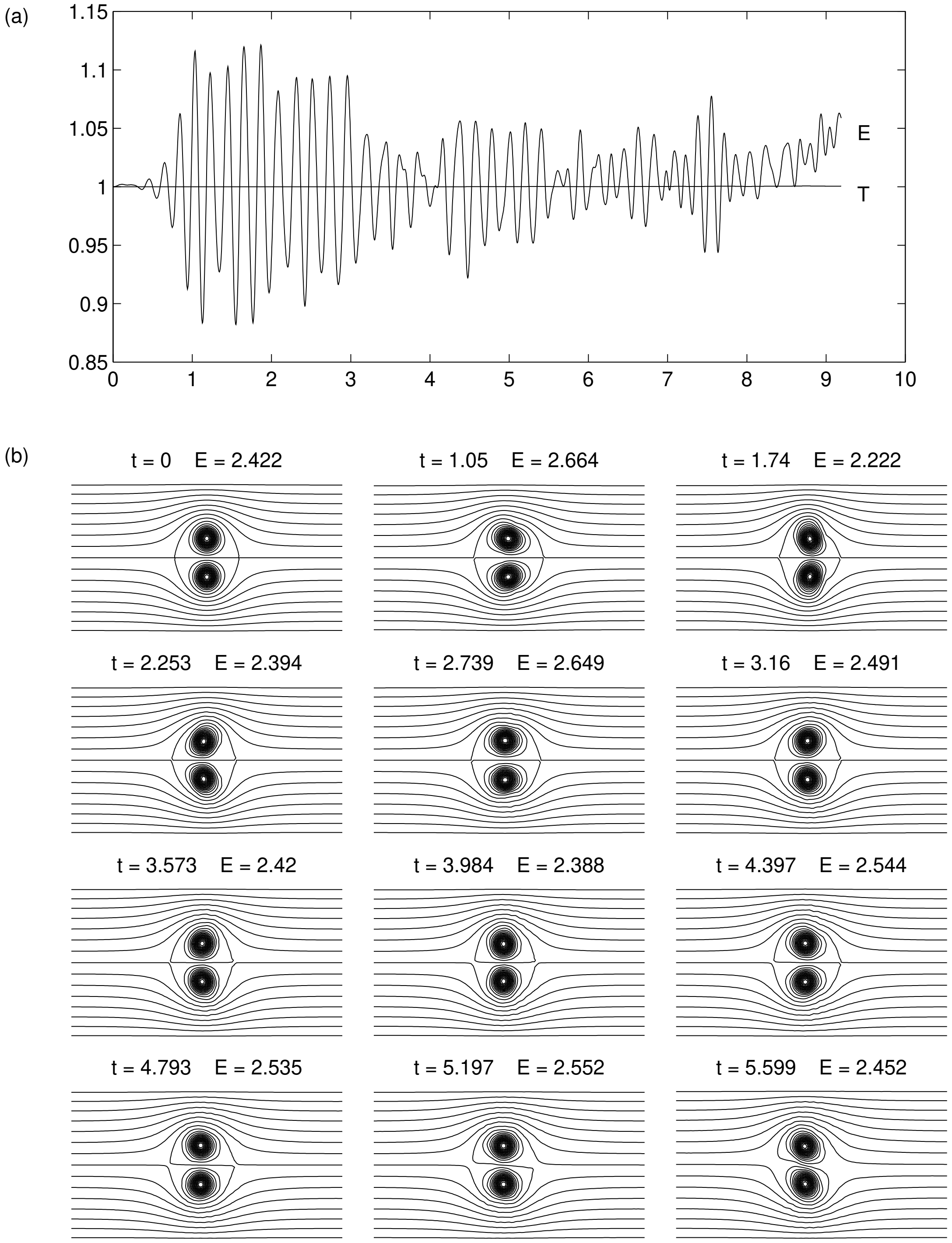

FIGURE 8. The behaviour of the near-equilibrium state in Case B under the Euler dynamics: (a) the kinetic energy E and the enstrophy T vary within 15% of their initial values; (b) snap-shots show that the modon initially oscillates and become unstable.

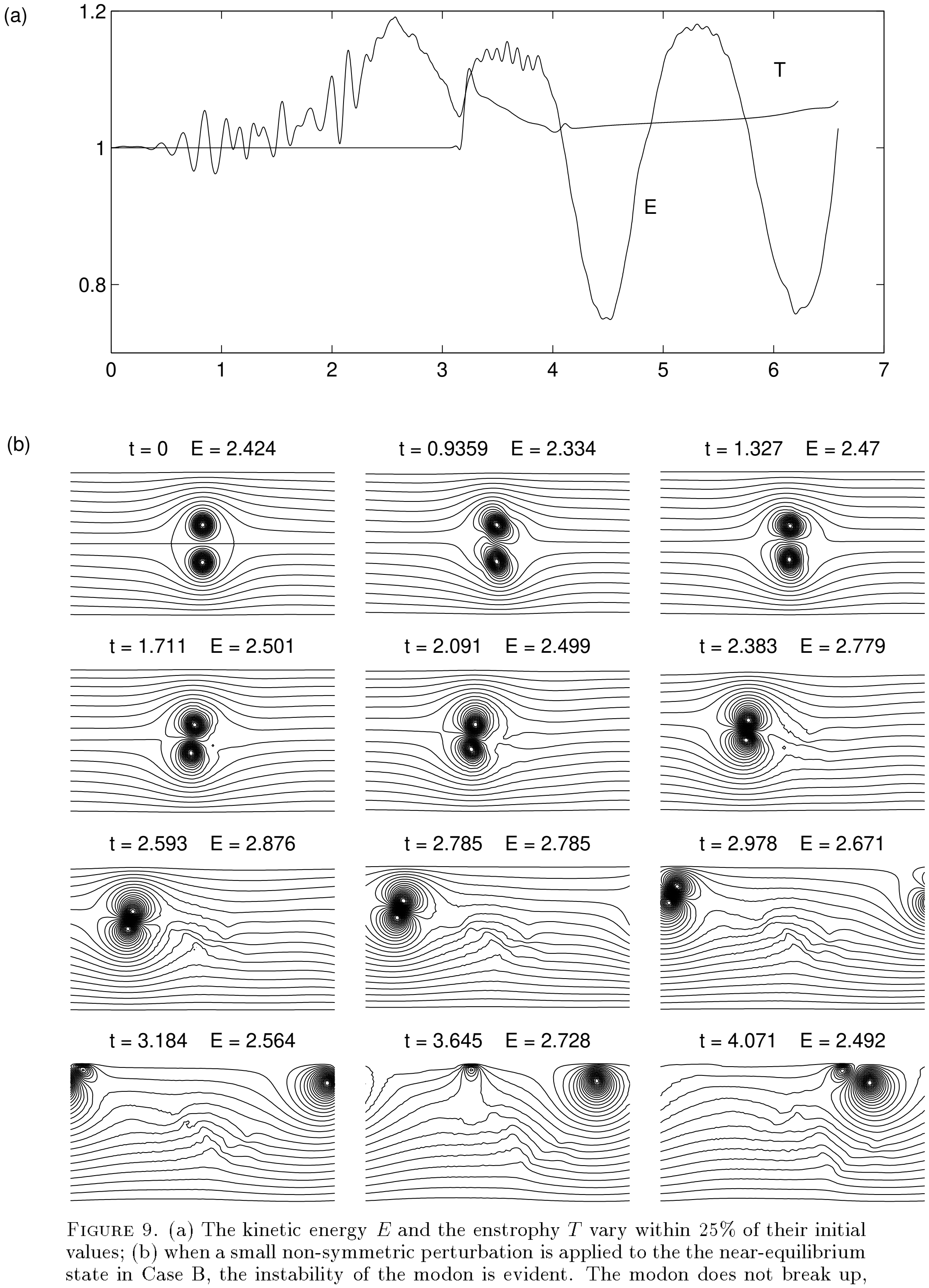

FIGURE 9. (a) The kinetic energy E and the enstrophy T vary within 25% of their initial values; (b) when a small non-symmetric perturbation is applied to the the near-equilibrium state in Case B, the instability of the modon is evident. The modon does not break up, but moves away from the centred position.

4. Discussion

In Boyd & Ma (1990), an elliptic modon is determined by first specifying its shape, and then evaluating the required circulation distribution. It is found that as such a modon becomes more elliptic, the circulation becomes stronger at its boundary. This phenomenon can now be explained physically via the magnetic analogy. Note that the magnetic field defined by the vector potential χ_A is concentrated near the boundary of the eddies. The magnetic pressure near the centre of the eddies is therefore low, and the eddies are liable to be compressed. The Lorentz force near the rigid walls pushes the fluid 'inwards' and thus the eddies are compressed in the y-direction (Figure 3).

The other case is also interesting. In case B, the magnetic field is concentrated near the centre of the eddies and the background field is relatively weak. The lines of magnetic force inside the eddies tend to be more circular and this dominating effect causes the eddies to elongate in the y-direction (Figure 2).

The unexpected non-symmetric instability can be interpreted as follows. Firstly, the two magnetic eddies repel each other because they behave like two parallel conducting elements carrying opposite current density (in the z-direction). Secondly, the background magnetic field has the effect of pushing the upper eddy downwards and the lower eddy upwards. When the magnetic modon is perturbed by a non-symmetric displacement, the torque generated by these magnetic forces rapidly tilts the modon.

It is worth noting that a similar tilting instability is also found in axisymmetric magnetic containment devices like SPHEROMAK. Rosenbluth & Bussac (1979) considered a force-free magnetic field $\mathbf{B}$ confined in a slightly perturbed spherical region, satisfying $\mathbf{j} = \nabla \wedge \mathbf{B} = k\mathbf{B}$ where k is a constant and has the same topology as a Hill's vortex. When the perturbation makes the sphere prolate (cf. Case A), an internal tilting instability (i.e. within the sphere) is found; when the perturbation makes the sphere oblate (cf. Case B), an external tilting mode is found unless the spherical region is bounded by a conducting shell of sufficiently small size. These results are very similar to ours, although the magnetostatic equilibria that we considered in this paper are two-dimensional and are not force-free.

To summarise, magnetic modons are in general non-circular, the direction of elongation of the eddies being different in the two cases considered. Numerical experiments have revealed that these magnetic modons are unexpectedly unstable: non-symmetric perturbation drives the structure to rotate, and reconnection takes place near the saddle points of the field due to (unavoidable) numerical diffusion. Eventually, the two magnetic eddies separate and they either hit the boundary or disappear altogether.

The near-equilibrium states referred to above are close to steady (analogous) Euler flows (or modons), whose stability has also been investigated numerically. Our results show that the modon may respond to disturbances in a manner similar to that of a perturbed Hill's vortex.

This work is supported by EPSRC under grant number GR/J21439 and UK/Hong Kong Joint Research Grant JRC 94/24.

REFERENCES

ARAKAWA, A. 1966 Computational Design for Long-Term Numerical Integration of the Equations of Fluid Motion: Two-Dimensional Incompress Flow. Part I. *J. Comp. Phys.* **1**, 119–143.

BOYD, J.P. & MA, H. 1990 Numerical study of elliptical modons using a spectral method. *J. Fluid Mech.* **221**, 597–611.

DAVIDSON, P.A. 1994 Global stability of two-dimensional and axisymmetric Euler flows. *J. Fluid Mech.* **276**, 273–306.

EYDELAND, A. & TURKINGTON, B. 1988 A computational method of solving free boundary problem in vortex dynamics. *J. Comp. Phys.* **78**, 194–214.

LINARDATOS, D. 1993 Determination of two-dimensional magnetostatic equilibria and analogous Euler flows. *J. Fluid Mech.* **246**, 569–591.

MOFFATT, H.K. 1985 Magnetostatic equilibria and analogous Euler flows of arbitrary complex topology. Part 1. Fundamentals. *J. Fluid Mech.* **159**, 359–378.

MOFFATT, H.K. 1986a On the existence of localized rotational disturbances which propagate without change of structure in an inviscid fluid. *J. Fluid Mech.* **173**, 289–302.

MOFFATT, H.K. 1986b Magnetostatic equilibria and analogous Euler flows of arbitrary complex topology. Part 2. Stability considerations. *J. Fluid Mech.* **166**, 359–378.

MOFFATT, H.K. & MOORE, D.W. 1978 The response of Hill's spherical vortex to a small axisymmetric disturbance. *J. Fluid Mech.* **87**, 749–760.

POZRIKIDIS, C. 1986 The nonlinear instability of Hill's vortex. *J. Fluid Mech.* **168**, 337–367.

ROSENBLUTH, M. N. AND BUSSAC, M. N. 1979 MHD stability of spheromak. *Nucl. Fusion* **19**, 489–498.